Article

Not peer-reviewed version

Exploring the Antibacterial and Antibiofilm Potential of Graphene Nanoparticles Synthesized from Candlenut Shell Waste

Muhammad Afiqamzar Azmi , Friscilla Romiduk Samosir , Anati Abd Rashid Syaida , Mohd Taufiq Mat Jalil , Norashirene Mohamad Jamil , Nurul Hidayah Mohamad Nor , Rikson Siburian * , Mohd Fakharul Zaman Raja Yahya *

Posted Date: 19 September 2025

doi: 10.20944/preprints202509.1635.v1

Keywords: biofilm; antibiofilm; graphene; candlenut shells; *Salmonella enteritidis; Staphylococcus aureus*

 doi:10.20944/preprints202509.1635.v1

Article

Exploring the Antibacterial and Antibiofilm Potential of Graphene Nanoparticles Synthesized from Candlenut Shell Waste

Muhammad Afiqamzar Azmi [1], Friscilla Romiduk Samosir [2], Anati Abd Rashid Syaida [1], Mohd Taufiq Mat Jalil [1], Norashirene Mohamad Jamil [1], Nurul Hidayah Mohamad Nor [3], Rikson Siburian [2,*] and Mohd Fakharul Zaman Raja Yahya [1,4,*]

[1] Faculty of Applied Sciences, Universiti Teknologi MARA, Shah Alam, Selangor, Malaysia
[2] Faculty of Mathematics and Natural Sciences, Universitas Sumatera Utara, Medan, Indonesia
[3] Low Dimensional Materials Research Centre, Faculty of Science, Universiti Malaya, Kuala Lumpur, Malaysia
[4] Integrative Pharmacogenomics Institute (iPROMISE), Puncak Alam, Selangor, Malaysia
* Correspondence: rikson@usu.ac.id (R.S.); fakharulzaman@uitm.edu.my (M.F.Z.R.Y.)

Abstract

The rising threat of antibiotic-resistant pathogens necessitates the development of novel antimicrobial agents, and graphene nanoparticles (GNPs) have emerged as a promising alternative due to their unique physicochemical properties. This study explores the antibacterial and antibiofilm efficacy of GNPs synthesized from candlenut shell waste (GNPsCSW) against *Staphylococcus aureus* and *Salmonella enteritidis*, addressing the unexplored potential of agro-waste-derived GNPs in combating bacterial infections. The GNPsCSW exhibited potent antibacterial activity, with MIC values of 12.5 µg/mL and 6.25 µg/mL against *S. aureus* and *S. enteritidis*, respectively, and MBC values of 25 µg/mL and 12.5 µg/mL, demonstrating superior bactericidal effects, particularly against *S. enteritidis*. Cell leakage assays revealed significant release of cellular materials (absorbance at 260 nm and 280 nm), confirming membrane disruption, while time-kill kinetics showed complete elimination of *S. aureus* within 12 hours at 25 µg/mL and rapid eradication of *S. enteritidis* within 8 hours at all tested concentrations. Biofilm assays demonstrated substantial inhibition of both biomass and viability biofilms, while FTIR spectroscopy revealed alterations in biofilm matrix composition, suggesting interference with extracellular polymeric substances. These results emphasize that GNPsCSW has both antibacterial and antibiofilm effects, offering a sustainable way to tackle resistant bacteria with consequences for both biomedical and environmental uses.

Keywords: biofilm; antibiofilm; graphene; candlenut shells; *Salmonella enteritidis*; *Staphylococcus aureus*

1. Introduction

Biofilm formation raises serious concerns in medical, industrial, and environmental contexts. It occurs when bacteria adhere to surfaces and, through quorum sensing, form highly resistant communities that are distinct from planktonic cells. These communities pose considerable public health risks, driving the search for novel antimicrobial agents [1]. Biofilms are protected by a matrix of extracellular matrix that shield them from nutritional limitations, antimicrobial treatments, and host immune responses [2]. Cells within biofilms exhibit unique genetic and phenotypic traits, making them significantly more resistant to harsh conditions than their planktonic counterparts. This elevated tolerance to antimicrobial drugs and immune defenses results in chronic and recurring infections that are notoriously difficult to treat [3]. The challenge of eradicating biofilm-associated infections is compounded by the ability of pathogens like Staphylococcus spp. and Salmonella spp. to withstand environmental stresses [4]. To address this, significant effort has been dedicated to developing biofilm-dispersing agents that revert colonized microbial cells to a more vulnerable

 doi:10.20944/preprints202509.1635.v1

planktonic state. Promising strategies include the use of enzymes such as glycoside hydrolases, proteases, and deoxyribonucleases that degrade the extracellular matrix, thereby increasing bacterial susceptibility to antimicrobial agents and host immune responses [5]. The clinical relevance of biofilms is underscored by their role in 65–80% of chronic and device-related infections, including catheter-associated urinary tract infections, chronic wounds, pneumonia, and infections of implants and prosthetic devices [6].

Given the urgent need for novel antimicrobial agents to combat biofilm-associated infections, attention has increasingly turned to natural products as promising alternatives. Among these is the candlenut (*Aleurites moluccana*), one of the six most valuable spices exported from Indonesia. It is a source of nutraceutical substances utilized as raw materials in the pharmaceutical and cosmetics sectors [7]. Candlenut has a long-standing history in folk medicine, documented both orally and in ancient written texts. Recent research has begun to elucidate the molecular and pharmacological mechanisms underlying its extensive traditional use. Extracts and secondary metabolites from this species have demonstrated intriguing biological activities, including cytotoxic, antibacterial, anti-inflammatory, and antinociceptive effects [8]. Beyond the nut itself, candlenut shells which are typically regarded as agricultural waste, have been investigated for their potential as a source of carbon-rich materials [9]. The shells possess a high fixed carbon content, making them suitable for conversion into advanced materials like graphene and biochar [10].

Graphene is a single-atom-thick sheet of carbon atoms arranged in a hexagonal lattice. It can be produced through various methods, including mechanical exfoliation and epitaxial growth, the latter showing promise for large-scale industrial production [11]. Graphene's exceptional properties, including an enormous surface area, make it valuable for energy storage applications such as supercapacitors and batteries [12]. Its biocompatibility and capacity for functionalization with various biomolecules also render it suitable for diverse biomedical applications, including tissue engineering, drug delivery systems, and biosensors [13]. Furthermore, graphene-based composites are advancing material science by enhancing material strength, demonstrating remarkable versatility across industries. However, further research is required to fully realize graphene's potential and optimize its performance in commercial products [14].

The antibacterial mechanisms of graphene-based materials include membrane disruption, oxidative stress, and the production of reactive oxygen species (ROS). These mechanisms are influenced by several factors, including the size, shape, concentration, and surface functional groups of the graphene material [15]. Graphene and its derivatives, such as graphene oxide (GO), can penetrate and damage microbial cell membranes. This occurs through strong interactions with membrane lipids, enabling graphene to extract phospholipids. This process compromises membrane integrity and reduces cell viability [16]. Graphene's sharp edges can physically pierce membranes, further enhancing its antibacterial properties [19]. This membrane damage can form pores, disrupting cellular homeostasis and leading to cell death [20]. Concurrently, graphene-based materials can induce oxidative stress by generating ROS, which cause damage to cellular components such as DNA, proteins, and lipids [19,20].

Significant antibiofilm effects have been demonstrated for GO. For instance, a GO-ZnO nanocomposite exhibited effective antibiofilm activity against *S. typhimurium*, inhibiting biofilm formation under both dark and visible light conditions [17]. In another study, GO at a concentration of 50 mg/L reduced *S. aureus* biofilm formation by 55.05% and decreased the viability of mature biofilms by 70.24% [18]. Furthermore, the selective bacterial inhibition achieved through functionalized graphene underscores its potential for developing targeted antibacterial therapies, leveraging its unique surface characteristics and chemical tunability [21]. Supported by advances in scalable production methods and a deeper understanding of its biological interactions, graphene-based antibacterial and antibiofilm treatments have the potential to revolutionize infection prevention and control. Therefore, this study aims to investigate the antibacterial and antibiofilm potential of graphene synthesized from candlenut shell waste against *S. aureus* and *S. enteritidis*.

 doi:10.20944/preprints202509.1635.v1

2. Materials and Methods

2.1. Graphene from Candlenut Shell Waste

The graphene sample was supplied by the Faculty of Natural Sciences and Mathematics at Universitas Sumatera Utara, Indonesia. Candlenut (A. moluccanus) shell wastes were used as the precursor in a two-step pyrolysis process to create graphene. To create charcoal chips, candlenut shells were pyrolyzed for five hours at 600 °C in a tube furnace with argon atmosphere. An equivalent amount of activated carbon was added to the charcoal chips to eliminate any functional groups generated from oxidation and the mixture was crushed. This mixture was pyrolyzed once more for one hour at 600 °C. The mixture was cooled, then rinsed with water and dried at 100–105 °C in an oven. To separate powdered graphene nanosheets from activated carbon, the dried mixture was ground up once more and filtered through a 200-mesh screen. Then, graphene nanoparticles from candlenut shell waste (GNPsCSW) were characterized using energy dispersive X-ray spectroscopy and scanning electron microscopy, SEM-EDX (JSM-7600F, JEOL, Tokyo, Japan), transmission electron microscopy, TEM (ACTEM JEOL JEM-ARM300F, JEOL, Tokyo, Japan), X-ray diffraction, XRD (LabX XRD-600, Shimadzu, Kyoto, Japan), Fourier transform infrared spectrometer, FTIR (Nicolet iS50 FTIR Spectrometer, Thermo, Wal-tham, MA, USA), and x-ray photoelectron spectrometer, XPS (XPS Kratos AXIS Supra, Shimadzu, Kyoto, Japan) [9].

2.2. Preparation of Test Microorganisms

Salmonella enterica serovar Enteritidis ATCC13076 and Staphylococcus aureus ATCC25923 were obtained from the Microbiology Laboratory, Faculty of Applied Science, Universiti Teknologi MARA (UiTM), Shah Alam, Malaysia. To evaluate the bacterial culture's purity, biochemical tests and Gram staining were carried out. At 37 °C, all microorganisms were cultured in nutrient broth. In the antibiofilm and broth microdilution tests, bacterial inocula having an optical density (OD) of 0.7 at 600 nm were used [22].

2.3. MIC and MBC Assays

Microbroth dilution method and resazurin dye were used to determine the minimum inhibitory concentrations (MIC) against the examined bacteria [23; 24]. Overnight-grown culture strains with a McFarland turbidity of 0.5 were cultivated on 96-well plates. Various doses of GNPsCSW (0.39, 0.78, 3.13, 6.25, 12.5, and 25 µg/mL) were tested. Ciprofloxacin (1 µg/mL) and 0.5% (v/v) DMSO served as the positive and negative controls, respectively, for both *S. aureus* and *S. enteritidis*. The plates were covered with plastic film and left to incubate for the entire night at 37 °C. The microplates were then filled with 30 µL of 0.02% (w/v) resazurin aqueous solution and incubated for two hours at 37 °C. The minimum inhibitory concentration (MIC) was defined as the lowest concentration that inhibited microbial growth, indicated by the absence of a color change in resazurin from blue to pink. The minimum bactericidal concentration (MBC) was determined by subculturing the contents of wells with concentrations at and above the MIC onto sterile Mueller-Hinton agar (MHA). The MBC was defined as the lowest concentration that resulted in no colony formation after incubation [24]. The MBC/MIC index was used to describe antibacterial activity. A MIC value of 1-2 indicates bactericidal activity, whereas a MIC index of 4-16 indicates bacteriostatic activity [25].

2.4. Cell Leakage Assay

The cell leakage assay was performed as previously described [26]. A bacterial pellet was obtained by centrifuging a suspension of cell biomass (18-24 hours) at 3500 rpm for 15-20 minutes, after which the supernatant was removed. The precipitate was collected and rinsed three times with a pH 7.4 phosphate buffer solution. It was then resuspended in the buffer before adding GNPsCSW at 0.39, 0.78, 3.13, 6.25, 12.5, and 25 µg/mL. The mixture was incubated at 37°C for 24 hours before being centrifuged for an additional 15 minutes at 3,500 rpm. Following the incubation time, the

 doi:10.20944/preprints202509.1635.v1

solutions were centrifuged for 15 minutes at 3500 rpm to extract the supernatant, and the pellet was discarded. The nucleic acid and protein content of the supernatant was evaluated using a Shimadzu UV-1800 UV-Vis Spectrophotometer (Shimadzu, Japan), which was used to collect the supernatant and measure cell leakage at 260 nm (nucleic acids) and 280 nm (proteins). The presence of bacterial membrane cell leakage was indicated by an increase in protein and nucleic acid content in the culture media, as measured by absorbance at their respective wavelengths.

2.5. Time-Kill Kinetics Assay

Time-kill kinetics assay was performed in accordance with [24]. Each strain's overnight-grown colonies were resuspended and incubated for two hours at 37 °C and 180 rpm. Each strain was inoculated into sterilized nutrient broth media with an inoculum size of 1×10^6 CFU/mL. Subsequent concentrations of GNPsCSW were then added, and the mixture was incubated at 37 °C at 180 rpm. There was also a growth control that had no GNPsCSW. At intervals of 0, 2, 4, 6, 8, and 16 hours, aliquots of 1 mL of cultures were extracted, spread out onto LB agar plates, and incubated for 24 hours at 37 °C. The number of viable cells was expressed as CFU/mL.

2.6. Antibiofilm Assay Using 96-Well Microplate

The antibiofilm activity of GNPsCSW was assessed using a 96-well microtiter plate biofilm assay, as described by [27]. Briefly, 100 µL of GNPsCSW at various concentrations (0.39, 0.78, 3.13, 6.25, 12.5, and 25 µg/mL) was mixed with 100 µL of an overnight bacterial culture in the wells of a 96-well plate. The plate was then incubated at 37 °C for 24 hours. After incubation, the contents of the wells were discarded, and the plates were gently rinsed twice with distilled water to remove non-adherent cells. For the biomass assay, the adherent biofilms were heat-fixed at 60 °C for 30 minutes and stained with 0.4% (w/v) crystal violet for 15 minutes. Following two rinses with distilled water to remove excess stain, the dye bound to the biofilm was solubilized by adding 200 µL of 95% (v/v) ethanol to each well. The absorbance of the solubilized crystal violet was then measured at 600 nm. For the viability assay, after rinsing, 200 µL of saline buffer was added to the wells to resuspend the biofilm cells. Then, 30 µL of a 0.02% (w/v) resazurin solution was added to each well. The plate was incubated at 37 °C for 2 hours or until a color change from blue to pink was observed. The absorbance was measured at 570 nm using a ThermoFisher Scientific microplate reader.

2.7. Antibiofilm Assay Using 6-Well Microplate

A 6-well microplate model was used to assess antibiofilm mode of action of GNPsCSW, as described by [28]. In short, a sterile 6-well microplate was pipetted with 2 mL of bacterial inoculum and GNPsCSW at different concentrations into each well. To create a surface for biofilm attachment, sterile glass coverslips were inserted into the wells. The plates were then incubated for 24 hours at 37 °C in an aerobic environment. The coverslips were heat-fixed at 60 °C for 30 minutes after being carefully rinsed with saline buffer to get rid of non-adherent cells.

2.8. Fourier-Transform Infrared (FTIR) Spectroscopy

Functional groups on the surface of the biofilm were identified using FTIR spectroscopy [29]. Glass coverslips from 6-well microplate were analyzed using FTIR spectroscopy Spectrum RXI system (PerkinElmer, Waltham, USA) at 8 cm^{-1} resolutions. All of the biofilms' spectra were captured in the 600–2000 cm^{-1} infrared wavelength range. Spectral data analysis, visualization, and processing were performed by using Perkin Elmer Applications Spectrum software. The structural and compositional changes in the biofilm extracellular matrix, initially indicated by FTIR spectroscopy, were further validated using quantitative spectrophotometric assays. To this end, an antibiofilm assay was performed in 6-well microplates as described above, but without sterile glass coverslips. Following incubation, the planktonic cells and culture medium were discarded, and the adherent biofilm cells were resuspended in saline buffer. The nucleic acid

 doi:10.20944/preprints202509.1635.v1

content was determined by measuring absorbance at 260 nm. The total protein and carbohydrate content were quantified using the Bradford assay (absorbance at 595 nm) and the phenol-sulfuric acid method (absorbance at 490 nm), respectively.

2.9. Statistical Analysis

The means ± standard deviation of at least three independent experiments (n=3) were used to represent all results from the cell leakage, crystal violet, resazurin, and biofilm matrix matrix assays. The significant difference between each test concentration and the control was assessed using the unpaired T-test. The threshold for statistical significance was set at $P < 0.05$. Strength of association between biofilm biomass and matrix components was determined using Pearson correlation coefficient test.

3. Results

3.1. MIC and MBC Values of GNPsCSW

The GNPsCSW exhibited potent antibacterial activity, with MIC values of 12.5 μg/mL and 6.25 μg/mL against *S. aureus* and *S. enteritidis*, respectively, and MBC values of 25 μg/mL and 12.5 μg/mL, demonstrating superior bactericidal effects (Table 1). The MIC and MBC results indicated that the GNPsCSW exhibited potent antibacterial activity against both the Gram-positive *S. aureus* and the Gram-negative *S. enteritidis. For* both pathogens, the MBC value was exactly twice the MIC value, a result that classifies the GNPsCSW as bactericidal against these strains. An MBC/MIC ratio of ≤ 4 is typically indicative of a bactericidal agent, meaning it kills bacteria rather than merely inhibiting their growth. The lower MIC value observed for *S. enteritidis* (6.25 μg/mL) compared to *S. aureus* (12.5 μg/mL) suggests the GNPsCSW is marginally more potent against this Gram-negative strain under the tested conditions. The consistent ratio of 2 for both organisms demonstrates a reliable and concentration-dependent killing effect, confirming the efficacy of GNPsCSW as a promising antibacterial agent with lethal action against both major classes of bacterial pathogens.

Table 1. MIC and MBC values of GNPsCSW against *S. aureus* and *S. enteritidis.*

Pathogens	MIC (μg/mL)	MBC(μg/mL)	MBC/MIC index
S. aureus	12.5	25	2
S. enteritidis	6.25	12.5	2

3.2. Bacterial Cell Leakage Following Treatment with GNPsCSW

The antibacterial efficacy of GNPsCSW against *S. aureus* and *S. enteritidis* was conclusively demonstrated by a significant, dose-dependent increase in the release of intracellular materials (Figure 2). The elevated levels of both nucleic acids and proteins detected in the supernatant, compared to the negative control, indicate severe damage to the integrity of the bacterial cell membrane. As the concentration of GNPsCSW increases, the corresponding rise in the leakage of these fundamental cellular components confirms a robust and concentration-dependent bactericidal mechanism, ultimately leading to cell lysis and death.

 doi:10.20944/preprints202509.1635.v1

A) S. aureus

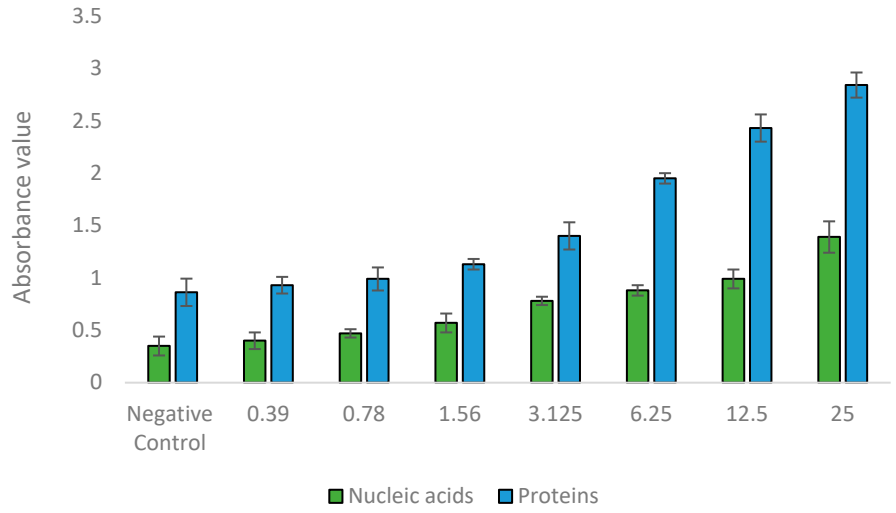

B) *S. enteritidis*

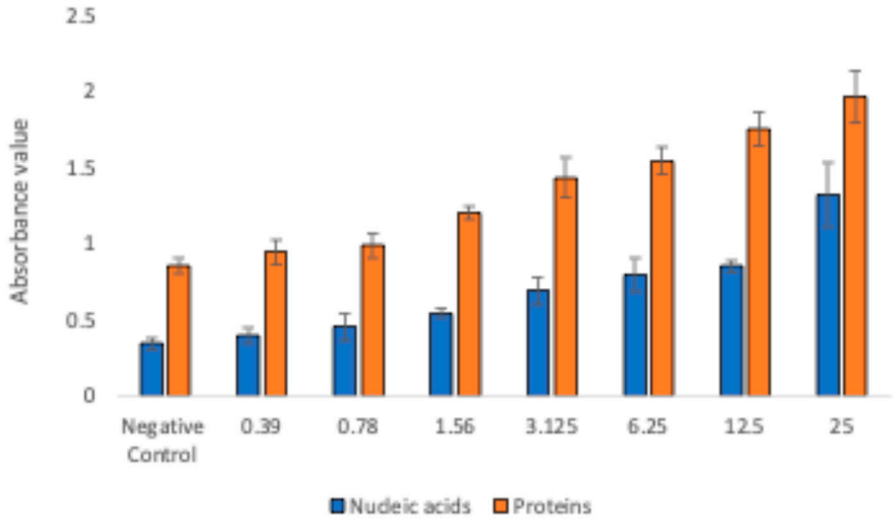

Figure 1. Release of cellular contents upon exposure to GNPsCSW.

3.3. Time-Kill Kinetics of GNPsCSW

Time-kill kinetics showed complete elimination of *S. aureus* within 12 hours at 25 μg/mL and rapid eradication of *S. enteritidis* within 8 hours at all tested concentrations of GNPsCSW (Figure 2). GNPsCSW demonstrated a clear concentration-dependent and time-dependent bactericidal effect against *S. aureus*. The control group (0 μg/mL) showed normal bacterial growth over time. As the concentration increased, the rate and extent of killing became more pronounced. At high concentrations (12.5–25 μg/mL), a significant reduction in bacterial count (log CFU/mL) was observed within the first eight hours, indicating rapid activity and strong potential as an antimicrobial agent. GNPsCSW also exerted a potent and concentration-dependent bactericidal effect against S. *enteritidis.* The control group (0 μg/mL) maintained robust bacterial growth over time, serving as a baseline. At the lowest concentration tested (0.39 μg/mL), a slight inhibitory effect was observed, manifesting as a reduced bacterial count compared to the control. This suppression becomes progressively more pronounced with increasing concentrations. The high concentrations (12.5 μg/mL and 25 μg/mL) exhibited the most dramatic efficacy, likely reducing the bacterial population by several orders of

 doi:10.20944/preprints202509.1635.v1

magnitude and potentially achieving complete or near-complete eradication within the assay period, which emphasize GNPsCSW's effective antimicrobial properties against this pathogen.

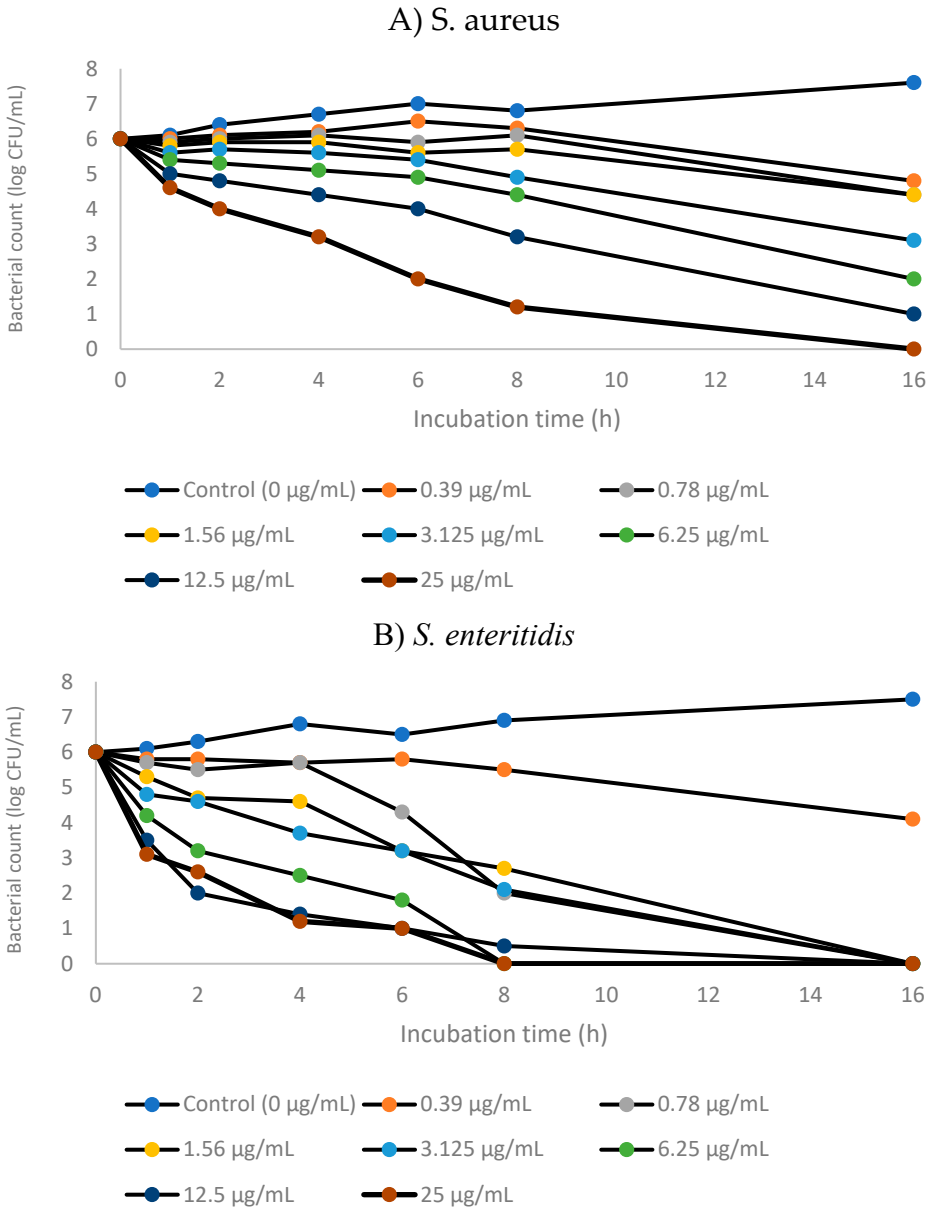

Figure 2. Time-kill kinetics of GNPsCSW against *S. aureus* and *S. enteritidis*.

3.4. Inhibitory Effects of GNPsCSW on Biomass and Viability of Biofilms

The effects of GNPsCSW on biofilm biomass and viability of *S. aureus* and *S. enteritidis* are shown in Figure 3. A significant reduction ($p<0.05$) in biofilm biomass was observed for both pathogens following treatment, with the inhibitory effect evident even at the lowest concentration tested. This reduction was consistent across all concentrations and statistically significant when compared with the untreated control. These findings indicate that GNPsCSW interferes with the establishment and maintenance of mature biofilm structures in both Gram-positive and Gram-negative bacteria.

In addition to biomass inhibition, a marked decline in biofilm viability was also detected in the presence of GNPsCSW. The decrease in viability was concentration-dependent, with higher concentrations producing more pronounced effects. Importantly, significant reductions ($p<0.05$) were observed at nearly all concentrations tested, highlighting the strong antimicrobial potential of the nanomaterial against biofilm-embedded cells. This dual action on biomass and viability suggests that

 doi:10.20944/preprints202509.1635.v1

GNPsCSW not only prevents biofilm formation but also compromises bacterial survival within the biofilm matrix.

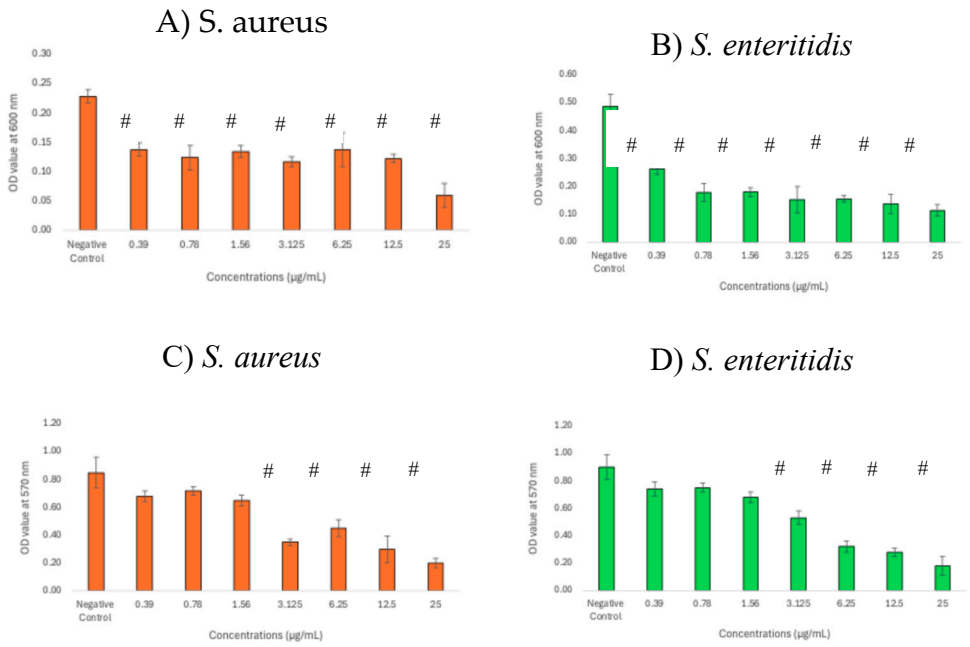

Figure 3. Biomass (A-B) and viability (C-D) of *S. aureus* and *S. enteritidis* biofilms in the presence of GNPsCSW. # indicates significant difference ($p<0.05$) as compared to negative control.

3.5. Structural Changes of Biofilms Following Treatment with GNPsCSW

GNPsCSW apparently reduced intensity of FTIR spectral peaks associated with the proteinaceous components of *S. aureus* biofilm was observed (Figure 4). Most notably, the peaks in the Amide I (~1630-1680 cm^{-1}) and Amide II (~1530-1550 cm^{-1}) spectral regions, which correspond to C=O stretching and N-H bending/C-N stretching in peptide backbones, respectively, showed a pronounced decrease in absorbance. This loss of signal intensity indicates extensive protein denaturation and degradation, likely affecting crucial bacterial enzymes, surface adhesins, and structural proteins that maintain biofilm integrity. Concurrently, the spectrum shows significant changes in the polysaccharide region. The intensity of peaks in the 1000-1100 cm^{-1} range, attributable to C-O-C and C-O-P stretching vibrations from glycosidic linkages in exopolysaccharides and cell wall teichoic acids, diminishes with increasing nanoparticle concentration. This indicates a direct disruptive effect on the polysaccharide scaffold of the biofilm matrix, which is essential for structural stability and cellular adhesion.

In *S. enteritidis* biofilm, the intensity of the Amide I band, located approximately between 1630 and 1680 cm^{-1} and originating from C=O stretching vibrations of peptide linkages, diminished considerably with increasing nanoparticle concentration (Figure 4). This reduction is accompanied by a similar decrease in the Amide II band (~1530-1550 cm^{-1}), which arises from N-H bending and C-N stretching vibrations. The attenuation of these two key amide peaks provides direct evidence of extensive protein denaturation and the hydrolysis of peptide bonds within the biofilm. This degradation likely affects critical structural proteins and enzymes necessary for biofilm stability and cellular function.

 doi:10.20944/preprints202509.1635.v1

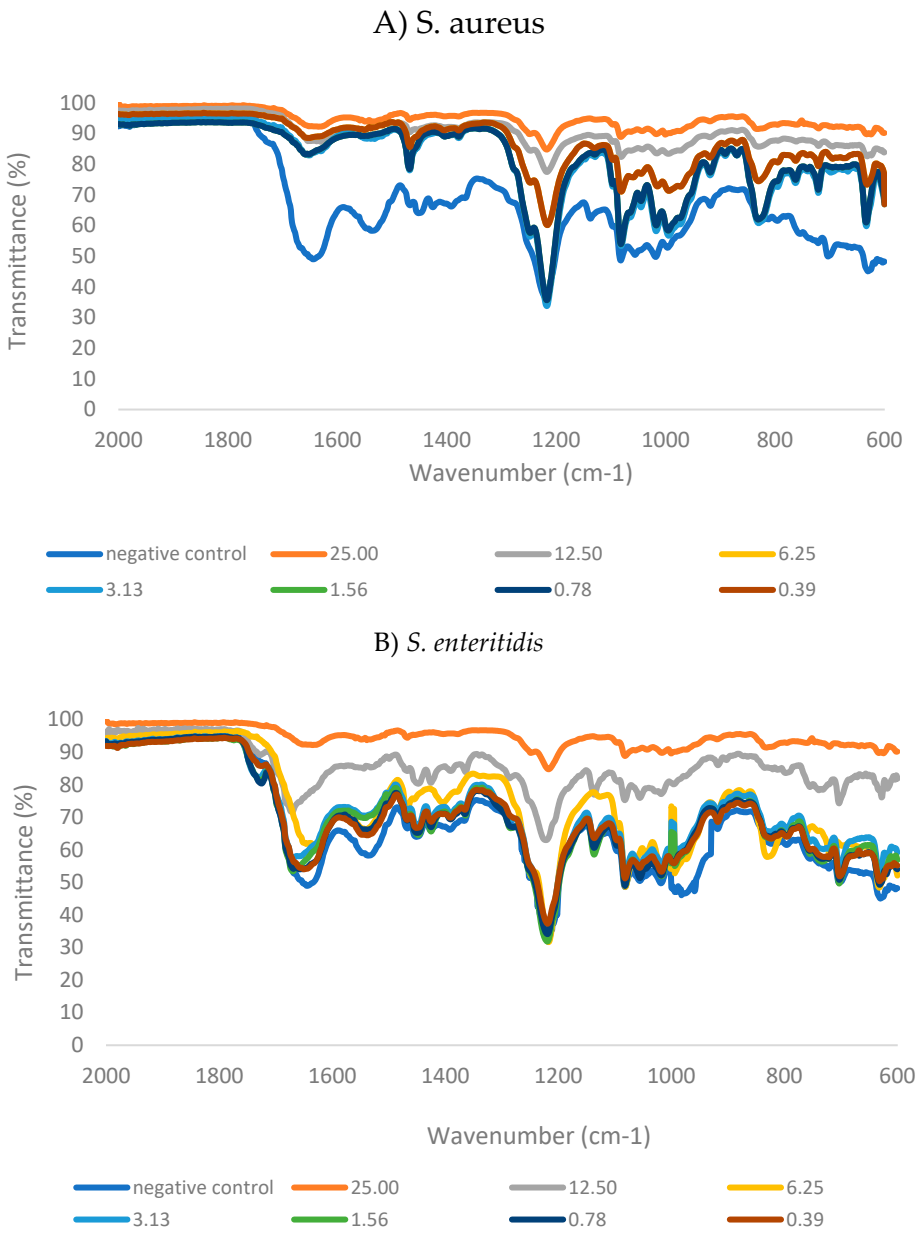

Figure 4. FTIR spectra of *S. aureus* and *S. enteritidis* in the presence of GNPsCSW. 1000-1100 cm^{-1}: C-O-C stretching (polysaccharide), P=O symmetric stretching (nucleic acids) [30]; 1530-1550 cm^{-1}: C=O stretching and N-H bending (Amide I, proteins) [31]; 1630-1680 cm^{-1}: N-H bending and C-N stretching (Amide II, proteins) [32].

3.6. Alteration of Biofilm Matrix Composition Following Treatment with GNPsCSW

The treatment with GNPsCSW demonstrated a significant and disruptive effect on the biofilm matrix of both *S. aureus* and *S. enteritidis* (Figure 5). Overall, the most substantial and significant reduction ($p<0.05$) in these matrix biomolecules was observed at the highest tested concentration of 25 μg/mL, suggesting that GNPsCSW exerts a potent disruptive effect on the biofilm architecture. The reduction in key biomolecules, namely carbohydrates, nucleic acids, and proteins, within the biofilm matrix indicates a potent antibiofilm mechanism. The observed reduction in these biomolecules correlated with a loss of biofilm biomass and viability, underscoring GNPsCSW's potential not only as an antibacterial agent but also as an effective strategy for combating biofilm-mediated resistance in both Gram-positive and Gram-negative pathogens.

 doi:10.20944/preprints202509.1635.v1

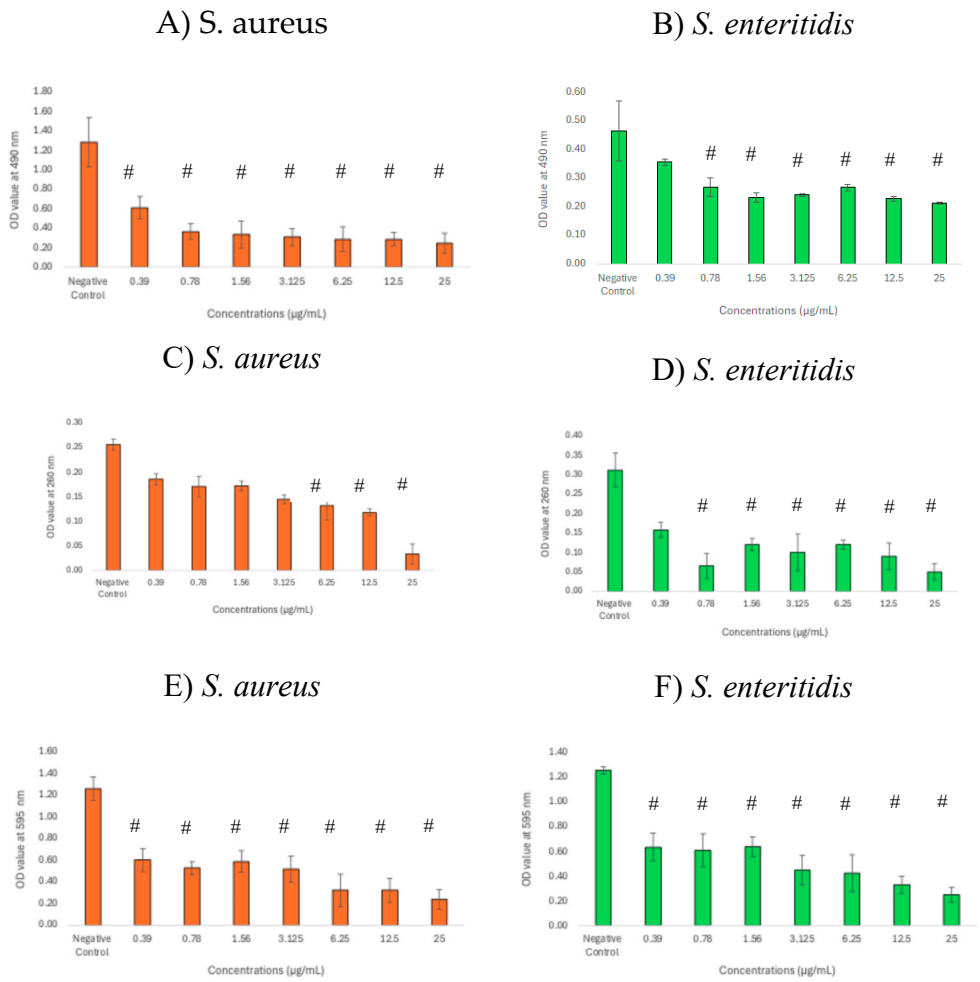

Figure 5. Reduction in biomolecules in biofilm matrix following treatment with GNPsCSW. A-B: carbohydrate; C-D: nucleic acids; E-F: proteins. # indicates significant difference ($p<0.05$) as compared to negative control.

3.7. Correlation Between Biofilm Biomass and Matrix Components

Based on the Pearson correlation coefficients (Table 2), a clear and striking dichotomy emerges between the mode of action of graphene against *S. aureus* and *S. enteritidis* biofilms. For both pathogens, the exceptionally high correlation values (all $r > 0.9$) indicate a strong, linear, proportional relationship between the reduction in total biofilm biomass and the reduction in each key matrix component namely carbohydrates, nucleic acids, and proteins. This strong correlation suggests that the primary mechanism of graphene's antibiofilm action against both species is a general, non-specific biocidal effect. The data implies that graphene treatment effectively kills the bacterial cells within the biofilm. Since dead and lysed cells cease to produce and maintain the extracellular matrix, the entire biofilm structure, including all its molecular components, collapses in proportion. The fact that all three matrix constituents are affected in lockstep with the biomass reduction indicates that graphene is not selectively targeting any specific matrix molecule but is rather causing a wholesale destruction of the biofilm community.

Table 2. Correlation between biofilms and their matrix components in the presence of GNPsCSW. B-C: biofilm biomass vs carbohydrates; B-NA: biofilm biomass vs nucleic acids; B-P: biofilm biomass vs proteins.

Relationships	*S. aureus*	*S. enteritidis*
B-C	0.877	0.971
B-NA	0.924	0.966
B-P	0.902	0.962

 doi:10.20944/preprints202509.1635.v1

4. Discussion

Candlenut shell waste represents a critically important and sustainable source for the production of graphene nanoparticles, aligning with the principles of green chemistry and waste valorization by transforming abundant, low-cost agricultural byproducts into high-value nanomaterials. The inherent lignocellulosic composition of candlenut shells, rich in sp^2-carbon precursors and natural hierarchical structures, provides an ideal foundation for efficient synthesis of graphene via pyrolysis [9].

In the present study, the lower MIC value observed for *S. enteritidis* (6.25 µg/mL) compared to *S. aureus* (12.5 µg/mL) suggests the GNPsCSW is marginally more potent against this Gram-negative strain under the tested conditions. The consistent ratio of 2 for both organisms demonstrates a reliable and concentration-dependent killing effect, confirming the efficacy of GNPsCSW as a promising antibacterial agent with lethal action against both major classes of bacterial pathogens. Graphene is hydrophobic and can interact with the hydrophobic components of bacterial membranes. The structural composition of Gram-negative bacteria like *S. enteritidis*, specifically their outer membrane rich in lipopolysaccharides, renders them more susceptible to graphene-induced damage compared to Gram-positive bacteria [33–36]. In addition, Karaky et al. [37] found that graphene alone exhibited a moderate level of antimicrobial efficacy (MIC = 62.5 mg/L) when compared to metal ions such as gold and palladium.

The cell leakage assay, which showed a significant increase in absorbance at 260 nm (nucleic acids) and 280 nm (proteins), provides direct mechanistic evidence for the primary mode of action of GNPsCSW namely massive membrane disruption and loss of membrane integrity. This is a hallmark of nanomaterial-mediated toxicity, particularly for sharp or sheet-like structures such as graphene [15,16,33,34]. The results confirm that the GNPsCSW does not merely inhibit metabolic pathways; it physically compromises the cell envelope, leading to the leakage of critical intracellular components. The efflux of nucleic acids and proteins is catastrophic for the cell, irrevocably leading to death. This physical mechanism is advantageous from a resistance standpoint, as bacteria are less likely to develop resistance against a physically destructive agent compared to a single-target biochemical inhibitor. The results align perfectly with the MBC data, explaining why the particles are bactericidal. Bacterial cell disruption and subsequent leaking of intracellular contents caused by graphene-based materials have also been reported elsewhere [38,39].

The time-kill kinetics study offers a dynamic view of the antibacterial efficacy, moving beyond a single time point. The rapid eradication of *S. enteritidis* within 8 hours at all tested concentrations underscores its susceptibility, consistent with the low MBC. The complete elimination of the more resilient *S. aureus* within 12 hours at 25 µg/mL is also impressive. This kinetic profile is crucial for developing optimal dosing strategies and guiding anti-infective drug development [40]. The faster action against *S. enteritidis* further reinforces the concept that its outer membrane is a key target, leading to a more rapid collapse of cellular integrity compared to the thicker cell wall of *S. aureus*. This suggestion aligns with De Moraes et al. [41] demonstrating that *E. coli* cells (Gram-negative) were completely inactivated by graphene oxide-silver nanocomposite (GO-Ag) approximately 2 hours earlier than MRSA cells (Gram-positive).

Biofilms are structured communities of bacteria encased in a self-produced matrix of extracellular polymeric substances and are notoriously resistant to conventional antibiotics [2,42]. The demonstration that GNPsCSW substantially inhibits both biomass formation and viability of biofilms suggests a dual functionality namely preventative action which can prevent the initial establishment of a biofilm, and eradicative action which can penetrate an existing biofilm matrix and kill embedded cells. Our findings corroborate Rosa et al. [43] reporting that graphene nanocoating significantly reduced metabolic activity, viable cell counts, and biofilm biomass of cross-kingdom biofilms of fungi and bacteria on titanium surfaces. Research shows that quantifying both biofilm biomass and viability is fundamentally important in antibiofilm studies because these two parameters provide distinct yet complementary information essential for evaluating the true efficacy of any potential treatment [29,44]. Measuring biomass reveals the total physical extent of the biofilm

 doi:10.20944/preprints202509.1635.v1

structure and the treatment's ability to disrupt its matrix, while assessing viability directly reports on the proportion of living cells within that structure that have been successfully killed or inhibited.

Fourier-transform infrared (FTIR) spectroscopy provided molecular-level insight into the mechanism of biofilm disruption because it provides a direct, biochemical snapshot of the structural and compositional changes induced within the biofilm matrix and the microbial cells themselves [29,30]. When an effective treatment is applied, FTIR can detect key spectral shifts indicative of mode of action, such as a reduction in polysaccharide-specific peaks, which points to the degradation of the extracellular polymeric substances (EPS) that provides the biofilm's structural integrity [45]. Simultaneously, changes in the amide I and II bands can reveal protein denaturation within the matrix or the cell membrane. In the present study, correlating these specific molecular-level alterations such as EPS degradation, protein misfolding, and membrane damage with observed biofilm dissolution and reduced viability, FTIR spectroscopy moves beyond simply confirming efficacy to providing a mechanistic rationale for how the treatment destabilizes the biofilm's architecture and compromises the viability of its embedded community.

Our data revealed alterations in the biofilm's biochemical composition, suggesting that GNPsCSW interferes with EPS components such as polysaccharides, proteins, and nucleic acids. The nanoparticles likely bind to and destabilize these matrix polymers, leading to disintegration of the biofilm's architectural integrity [46,47]. This breakdown of the protective EPS matrix presumably facilitates nanoparticle penetration to the underlying bacterial cells, where they can exert their membrane-disrupting effects. This two-pronged attack strategy, first dismantling the biofilm fortress and then attacking the encapsulated cells, explains the observed excellent antibiofilm activity and highlights the multi-targeted mechanism of GNPsCSW. Supporting this approach, Jiang et al. [48] demonstrated that FTIR spectroscopy effectively detected structural changes in protein secondary structure and decrease in β-sheet/α-helix ratios following exposure to Al_2O_3, TiO_2, and ZnO nanoparticles. Similarly, Sportelli et al. [49] reported changes in the Amide I and Amide II spectral regions of *Pseudomonas fluorescens* biofilm after interaction with Ag-CFx nanocomposites. To the best of our knowledge, this is the first effort to provide a mechanistic, composition-centric understanding of how biofilms from these two clinically relevant pathogens respond to, and are compromised by, graphene nanomaterial synthesized from candlenut shell waste.

Strong, linear, proportional relationships between the reduction in total biofilm biomass and the reduction in each key matrix component were observed in *S. aureus* and *S. enteritidis* following exposure to GNPsCSW. A subtle but potentially significant difference between the two bacteria can be observed. The correlation coefficients for *S. enteritidis* are consistently and slightly higher (0.971, 0.966, 0.962) than those for *S. aureus* (0.877, 0.924, 0.902). This indicates that the relationship between cell death and matrix degradation is even more tightly coupled in *S. enteritidis*. The marginally lower values for *S. aureus*, particularly for the biomass vs. carbohydrates correlation, could hint at a minor secondary mechanism or a slight difference in the timing of the matrix disruption. It may suggest that the *S. aureus* matrix may offer a small degree of initial buffering or undergoes a marginally different degradation process upon GNPsCSW treatment, supporting the time-kill kinetics results mentioned earlier. Linear and proportional relationships between the reduction in total biofilm biomass and the reduction in EPS proteins in the presence of antibiofilm compound have been reported by Yahya et al. [30]. One study on *Pseudomonas aeruginosa* biofilms demonstrated that treatments reducing quorum sensing (QS) signals led to decreased EPS content, including proteins, which corresponded to lower total biofilm biomass, indicating the tight linkage between EPS protein reduction and biofilm dispersal [50]. In this study, the addition of QS interfering compounds reduced EPS concentration substantially alongside biofilm biomass, revealing the impact of EPS components on biofilm stability. Joos et al. [51] also demonstrated that, in Salmonella biofilms treated with EPS inhibitors, evolved populations exhibited reduced biofilm biomass and decreased expression of key biofilm regulators, which correlated with diminished EPS production including protein components, resulting in less biofilm formation. Collectively, the research underscores that EPS proteins are integral to biofilm matrix cohesion, and their reduction parallels biofilm biomass decrease.

 doi:10.20944/preprints202509.1635.v1

5. Conclusions

This study highlights the antibacterial and antibiofilm activity of graphene nanoparticles synthesized from candlenut shells waste (GNPsCSW) against *S. aureus* and S. *enteritidis*. Graphene's antibiofilm effects underscore its potential as a component in novel therapeutic strategies against biofilm-associated infections, and its eco-friendly production from waste sources adds to its industrial and environmental appeal. Future studies should explore graphene's long-term efficacy and safety in biomedical applications.

Author Contributions: Conceptualization, R.S. and M.F.Z.R.Y.; methodology, M.A.A., F.R.S., A.A.R.S.; validation, M.F.Z.R.Y, M.T.M.J. and N.M.J.; formal analysis, M.A.A., A.A.R.S., M.F.Z.R.Y.; resources, R.S., M.F.Z.R.Y.; writing—original draft preparation, M.A.A., A.A.R.S.; writing—review and editing, M.F.Z.R.Y. N.H.M.N.; supervision, R.S., M.F.Z.R.Y.; funding acquisition, R.S. All authors have read and agreed to the published version of the manuscript. .

Funding: This research was funded by Universitas Sumatera Utara, grant number 600-TNCPI/PBT 5/3 INT (036/2025).

Conflicts of Interest: The authors declare no conflict of interest.

Abbreviations

The following abbreviations are used in this manuscript:

GNPs	Graphene nanoparticles
GNPsCSW	Graphene nanoparticles synthesized from candlenut shell waste
MIC	Minimum inhibitory concentration
MBC	Minimum bactericidal concentraion
FTIR	Fourier-transform infrared

References

1. Fathima, A., Arafath, Y., Hassan, S., Prathiviraj, R., Kiran, G. S., & Selvin, J. Microbial biofilms: A persisting public health challenge. In *Understanding Microbial Biofilms* **2023**, (pp. 291–314). [
2. Malakar, C., Deka, S., & Kalita, M. C. Role of biosurfactants in biofilm prevention and disruption. In *Advancements in Biosurfactants Research* **2023** (pp. 481–501).
3. Baishya, J., Everett, J. A., Chazin, W. J., Rumbaugh, K. P., & Wakeman, C. A. The innate immune protein calprotectin interacts with and encases biofilm communities of *Pseudomonas aeruginosa* and *Staphylococcus aureus*. *Frontiers in Cellular and Infection Microbiology* **2022**, *12*.
4. Scaffo, J., Lima, R., Dobrotka, C., Ribeiro, T., Pereira, R., Sachs, D., Ferreira, R., & Aguiar-Alves, F. In vitro analysis of interactions between *Staphylococcus aureus* and *Pseudomonas aeruginosa* during biofilm formation. *Antibiotics* **2025**, *14*, 504.
5. Wang, S., Zhao, Y., Breslawec, A., Liang, T., Deng, Z., Kuperman, L., & Yu, Q. Strategy to combat biofilms: a focus on biofilm dispersal enzymes. *NPJ Biofilms and Microbiomes* **2023**, *9*, 63.
6. Li, P., Yin, R., Cheng, J., & Lin, J. Bacterial biofilm formation on biomaterials and approaches to its treatment and prevention. *Int. J. Mol. Sci.* **2023**, *24*, 11680.
7. Shintawati, N., Widodo, Y., & Ermaya, D. Yield and quality improvement of candlenut oil by microwave assisted extraction (MAE) methods. *IOP Conference Series Earth and Environmental Science* **2022**, 1012(1), 012024.
8. Hakim, A., Jamaluddin, J., Idrus, S. W. A., Jufri, A. W., & Ningsih, B. N. S. Ethnopharmacology, phytochemistry, and biological activity review of *Aleurites moluccana*. *J Appl Pharm Sci* **2022**, *12*, 170–*178*.

 doi:10.20944/preprints202509.1635.v1

9. Siburian, R., Tarigan, K., Manik, Y. G. O., Hutagalung, F., Alias, Y., Chan, Y. C., Chang, B. P., Siow, J., Ong, A. J., Huang, J., Paiman, S., Goh, B. T., Simatupang, L., Goei, R., Tok, A. I. Y., Yahya, M. F. Z. R., & Bahfie, F. Converting candlenut shell waste into graphene for electrode applications. *Processes* **2024**, *12*, 1544.
10. Lempang, M., Sallata, M. K., & Ansari, F. Modified drum kiln application to produce candlenut shell charcoal as alternative bioenergy. *AIP Conference Proceedings* **2025**, 3285, 020003.
11. Neto, A. C., Guinea, F., & Peres, N. M. Drawing conclusions from graphene. *Physics World* **2006**, *19*(11), 33–37.
12. Muthuvinayagam, M., Kumar, S. S. A., Ramesh, K., & Ramesh, S. Introduction of graphene: the "Mother" of all carbon allotropes. In *Engineering materials* **2023**, (pp. 5–20).
13. Kaur, H., Garg, R., Singh, S., Jana, A., Bathula, C., Kim, H., Kumbar, S. G., & Mittal, M. Progress and challenges of graphene and its congeners for biomedical applications. *Journal of Molecular Liquids* **2022**, *368*, 120703.
14. Abdulqader, A. F., Salman, L. B., Nasr, Y. F., Bodnar, N., & Hikmat, R. Graphene based composites material characteristics and industrial uses. *Radioelectronics Nanosystems Information Technologies* **2024**, *16*, 605–616.
15. Seifi, T., & Kamali, A. R. Anti-pathogenic activity of graphene nanomaterials: A review. *Colloids and Surfaces B: Biointerfaces* **2021**, *199*, 111509.
16. Tu, Y., Lv, M., Xiu, P., Huynh, T., Zhang, M., Castelli, M., Liu, Z., Huang, Q., Fan, C., Fang, H., & Zhou, R. Destructive extraction of phospholipids from *Escherichia coli* membranes by graphene nanosheets. *Nature Nanotechnology* **2013**, *8*, 594–601.
17. Prema, D., Binu, N. M., Prakash, J., & Venkatasubbu, G. D. Photo induced mechanistic activity of GO/Zn(Cu)O nanocomposite against infectious pathogens: Potential application in wound healing. *Photodiagnosis and Photodynamic Therapy* **2021**, *34*, 102291.
18. Di Giulio, M., Di Lodovico, S., Fontana, A., Traini, T., Di Campli, E., Pilato, S., D'Ercole, S., & Cellini, L. Graphene oxide affects *Staphylococcus aureus* and *Pseudomonas aeruginosa* dual species biofilm in Lubbock chronic wound biofilm model. *Scientific Reports* **2020**, *10*, 18525.
19. Er, S. G., Edirisinghe, M., & Tabish, T. A. Graphene--Based nanocomposites as antibacterial, antiviral and antifungal agents. *Advanced Healthcare Materials* **2023**, *12*, 2201523.
20. Pham, V. T. H., Truong, V. K., Quinn, M. D. J., Notley, S. M., Guo, Y., Baulin, V. A., Kobaisi, M. A., Crawford, R. J., & Ivanova, E. P. Graphene induces formation of pores that kill spherical and Rod-shaped bacteria. *ACS Nano* **2015**, *9*(8), 8458–8467.
21. Zheng, A. L. T., Farrag, H. N., Sabidi, S., Kato, T., Maeda, T., & Andou, Y. Accessing the anti-microbial activity of cyclic peptide immobilized on reduced graphene oxide. *Materials Letters* **2021**, *304*, 130621.
22. Amran, S.S.D., Jalil, M.T.M., Aziz, A.A., Yahya, M.F.Z.R.Y. Methanolic extract of *Swietenia macrophylla* exhibits antibacterial and antibiofilm efficacy against Gram-positive pathogens. *Malaysian Applied Biology* **2023**, *52*, 129-138.
23. Shehabeldine, A.M., Amin, B.H., Hagras, F.A. Potential antimicrobial and antibiofilm properties of copper oxide nanoparticles: Time-kill kinetic essay and ultrastructure of pathogenic bacterial cells. *Appl Biochem Biotechnol* **2023**, *195*, 467–485.
24. Caso Coelho, V., Pereira Neves, S. D. A., CintraGiudice, M., Benard, G., Lopes, M. H., & Sato, P. K. Evaluation of antimicrobial susceptibility testing of *Nocardia* spp. isolates by broth microdilution with resazurin and spectrophotometry. *BMC Microbiology* **2021**, 21, 1–8.
25. Hasanin, M., Elbahnasawy, M. A., Shehabeldine, A. M., & Hashem, A. H. Ecofriendly preparation of silver nanoparticles-based nanocomposite stabilized by polysaccharides with antibacterial, antifungal and antiviral activities. *BioMetals* **2021**, *34*, 1313–1328.

 doi:10.20944/preprints202509.1635.v1

26. Abdullah, M.I., Yahya, M.F.Z.R., Bakar, L.M., Zakaria, N.A., Ibrahim, D. & Mat Jalil, M.T. Efficacy of *Terminalia catappa* leaves extract as an antimicrobial agent against pathogenic bacteria. *Malaysian Applied Biology* **2024**, *53*, 35-47.
27. Okba, M. M., Baki, P. M. A., Abu-Elghait, M., Shehabeldine, A. M., El-Sherei, M. M., Khaleel, A. E., & Salem, M. A. UPLC-ESI-MS/MS profiling of the underground parts of common Iris species in relation to their anti-virulence activities against *Staphylococcus aureus*. *Journal of Ethnopharmacology* **2022**, *282*, 114658.
28. Amran, S. S. D., Syaida, A. A. R., Jalil, M. T.M., Nor, N. H. M., & Yahya, M. F. Z. R. Preparation of biofilm assay using 96-well and 6-well microplates for quantitative measurement and structural characterization: A review. *Science Letters* **2024**. *18*. 121-134.
29. Johari, N. A., Aazmi, M. S., & Yahya, M. F. Z. R. FTIR spectroscopic study of inhibition of chloroxylenol-based disinfectant against *Salmonella enterica* serovar Thyphimurium biofilm. *Malaysian Applied Biology* **2023**, *52*(2), 97–107. [Google Scholar]
30. Yahya, M. F. Z. R., Alias, Z., & Karsani, S. A. Antibiofilm activity and mode of action of DMSO alone and its combination with afatinib against Gram-negative pathogens. *Folia Microbiologica* **2018**, *63*(1), 23-30.
31. Biswas, D., Tiwari, M., & Tiwari, V. Molecular mechanism of antimicrobial activity of chlorhexidine against carbapenem-resistant *Acinetobacter baumannii*. *PloS one* **2019**, *14*(10), e0224107.
32. DeQueiroz, G. A., & Day, D. F. Antimicrobial activity and effectiveness of a combination of sodium hypochlorite and hydrogen peroxide in killing and removing *Pseudomonas aeruginosa* biofilms from surfaces. *Journal of Applied Microbiology* **2007**, *103*(4), 794-802.
33. Duan, G., Zhang, Y., Luan, B., Weber, J. K., Zhou, R. W., Yang, Z., ... & Zhou, R. Graphene-induced pore formation on cell membranes. *Scientific Reports* **2017**, *7*(1), 42767.
34. Tu, Y., Lv, M., Xiu, P., Huynh, T., Zhang, M., Castelli, M., ... & Zhou, R. Destructive extraction of phospholipids from Escherichia coli membranes by graphene nanosheets. *Nature nanotechnology* **2013**, *8*(8), 594-601.
35. Lundstedt, E., Kahne, D., & Ruiz, N. Assembly and maintenance of lipids at the bacterial outer membrane. *Chemical reviews* **2020**, *121*(9), 5098-5123.
36. Tan, K. H., Sattari, S., Beyranvand, S., Faghani, A., Ludwig, K., Schwibbert, K., ... & Adeli, M. Thermoresponsive amphiphilic functionalization of thermally reduced graphene oxide to study graphene/bacteria hydrophobic interactions. *Langmuir* **2019**, *35*(13), 4736-4746.
37. Karaky, N., Tang, S., Ramalingam, P., Kirby, A., McBain, A. J., Banks, C. E., & Whitehead, K. A. Multidrug-Resistant Escherichia coli Remains Susceptible to Metal Ions and Graphene-Based Compounds. *Antibiotics* **2024**, *13*(5), 381.
38. Wong, F., Stokes, J. M., Cervantes, B., Penkov, S., Friedrichs, J., Renner, L. D., & Collins, J. J. Cytoplasmic condensation induced by membrane damage is associated with antibiotic lethality. *Nature communications* **2021**, *12*(1), 2321.
39. Elbasuney, S., Yehia, M., Ismael, S., Al-Hazmi, N. E., El-Sayyad, G. S., & Tantawy, H. Potential impact of reduced graphene oxide incorporated metal oxide nanocomposites as antimicrobial, and antibiofilm agents against pathogenic microbes: Bacterial protein leakage reaction mechanism. *Journal of Cluster Science* **2023**, *34*(2), 823-840.
40. Vaddady, P. K., Lee, R. E., & Meibohm, B. In vitro pharmacokinetic/pharmacodynamic models in anti-infective drug development: focus on TB. *Future Medicinal Chemistry* **2010**, *2*(8), 1355-1369.
41. De Moraes, A. C. M., Lima, B. A., de Faria, A. F., Brocchi, M., & Alves, O. L. Graphene oxide-silver nanocomposite as a promising biocidal agent against methicillin-resistant Staphylococcus aureus. *International Journal of Nanomedicine* **2015**, 6847-6861.

 doi:10.20944/preprints202509.1635.v1

42. Yahya, M. F. Z. R., Jalil, M. T. M., Jamil, N. M., Nor, N. H. M., Alhajj, N., Siburian, R., & Majid, N. A. Biofilms and multidrug resistance: an emerging crisis and the need for multidisciplinary interventions. *Frontiers in Bioengineering and Biotechnology* **2025**, *13*, 1625356.
43. Rosa, V., Vidhawan, A. S., Seneviratne, C. J., & Silikas, N. Graphene nanocoating inhibits cross-kingdom biofilms on titanium. *Dental Materials* **2023**, 39, e61.
44. Kamaruzzaman, A. N. A., Mulok, T. E. T. Z., & Yahya, M. F. Z. R. Inhibitory action of topical antifungal creams against Candida albicans biofilm. *Journal of Sustainability Science and Management* **2022**, *17*(2), 27-34.
45. Nag, M., Lahiri, D., Banerjee, R., Chatterjee, A., Ghosh, A., Banerjee, P., & Ray, R. R. Analysing Microbial Biofilm Formation at a Molecular Level: Role of Fourier Transform Infrared and Raman Spectroscopy **2021.** In Analytical Methodologies for Biofilm Research (pp. 69-93). New York, NY: Springer US.
46. Abriat, C., Gazil, O., Heuzey, M. C., Daigle, F., & Virgilio, N. The polymeric matrix composition of Vibrio cholerae biofilms modulate resistance to silver nanoparticles prepared by hydrothermal synthesis. *ACS Applied Materials & Interfaces* **2021**, *13*(30), 35356-35364.
47. Qayyum, S., & Khan, A. U. Nanoparticles vs. biofilms: a battle against another paradigm of antibiotic resistance. *MedChemComm* **2016**, *7*(8), 1479-1498.
48. Jiang, W., Yang, K., Vachet, R. W., & Xing, B. Interaction between oxide nanoparticles and biomolecules of the bacterial cell envelope as examined by infrared spectroscopy. *Langmuir* **2010**, *26*(23), 18071-18077.
49. Sportelli, M. C., Tütüncü, E., Picca, R. A., Valentini, M., Valentini, A., Kranz, C., ... & Cioffi, N. Inhibiting P. fluorescens biofilms with fluoropolymer-embedded silver nanoparticles: an in-situ spectroscopic study. *Scientific reports* **2017**, *7*(1), 11870.
50. Song, W., Ryu, J., Jung, J., Yu, Y., Choi, S., & Kweon, J. Dispersive biofilm from membrane bioreactor strains: effects of diffusible signal factor addition and characterization by dispersion index. *Frontiers in Microbiology* **2023**, *14*, 1211761.
51. Joos, M., Van Ginneken, S., Villanueva, X., Dijkmans, M., Coppola, G. A., Pérez-Romero, C. A., ... & Steenackers, H. P. EPS inhibitor treatment of Salmonella impacts evolution without selecting for resistance to biofilm inhibition. *npj Biofilms and Microbiomes* **2025**, *11*(1), 73.